NMR Solution Structure of a Complex of Calmodulin with a Binding Peptide of the Ca^{2+} Pump[†,‡]

Bettina Elshorst,[§] Mirko Hennig,[§] Holger Försterling,[§] Alexander Diener,[§] Marcus Maurer,[§] Petra Schulte,[§] Harald Schwalbe,[§] Christian Griesinger,*[,§] Joachim Krebs,*[,||] Holger Schmid,[||,⊥] Thomas Vorherr,[||,⊥] and Ernesto Carafoli[||,#]

Institute of Organic Chemistry, University of Frankfurt, D-60439 Frankfurt, Germany, and Institute of Biochemistry, Swiss Federal Institute of Technology (ETH), CH-8092 Zurich, Switzerland

Received April 8, 1999; Revised Manuscript Received June 25, 1999

ABSTRACT: The three-dimensional structure of the complex between calmodulin (CaM) and a peptide corresponding to the N-terminal portion of the CaM-binding domain of the plasma membrane calcium pump, the peptide C20W, has been solved by heteronuclear three-dimensional nuclear magnetic resonance (NMR) spectroscopy. The structure calculation is based on a total of 1808 intramolecular NOEs and 49 intermolecular NOEs between the peptide C20W and calmodulin from heteronuclear-filtered NOESY spectra and a half-filtered experiment, respectively. Chemical shift differences between free Ca^{2+}-saturated CaM and its complex with C20W as well as the structure calculation reveal that C20W binds solely to the C-terminal half of CaM. In addition, comparison of the methyl resonances of the nine assigned methionine residues of free Ca^{2+}-saturated CaM with those of the CaM/C20W complex revealed a significant difference between the N-terminal and the C-terminal domain; i.e., resonances in the N-terminal domain of the complex were much more similar to those reported for free CaM in contrast to those in the C-terminal half which were significantly different not only from the resonances of free CaM but also from those reported for the CaM/M13 complex. As a consequence, the global structure of the CaM/C20W complex is unusual, i.e., different from other peptide calmodulin complexes, since we find no indication for a collapsed structure. The fine modulation in the peptide protein interface shows a number of differences to the CaM/M13 complex studied by Ikura et al. [Ikura, M., Clore, G. M., Gronenborn, A. M., Zhu, G., Klee, C. B., and Bax, A. (1992) *Science 256*, 632−638]. The unusual binding mode to only the C-terminal half of CaM is in agreement with the biochemical observation that the calcium pump can be activated by the C-terminal half of CaM alone [Guerini, D., Krebs, J., and Carafoli, E. (1984) *J. Biol. Chem. 259*, 15172−15177].

Calcium plays a central role in the modulation of a number of cellular processes (*1*). The receptor protein that mediates the calcium signal to most intracellular targets is calmodulin (CaM)[1] (for review see ref *2*). The binding of Ca^{2+} alters the conformation of CaM, exposing hydrophobic patches (*3*−*5*) on its surface and thereby conferring to CaM the ability to interact with intracellular targets.

The X-ray structure of Ca^{2+}-loaded CaM reveals an extended, rigid, and dumbbell shape, in which the two domains are connected by a rigid α-helix (Figure 1a). ^{15}N relaxation studies (*6*), hydrogen exchange rates, and chemical shift perturbations (*7*) of the protein in solution suggest that the central part of this long stretched helix (Asp78 through Ser81) is disordered and, therefore, the two domains show no conserved relative orientation; i.e., in solution this central helix is a "flexible tether" (*8*).

The structures of Ca^{2+}-loaded CaM complexed to binding peptides derived from skeletal and smooth muscle myosin light chain kinase (MLCK) and from CaM kinase IIα (CaMKIIα) have been solved by NMR (*9*) and by X-ray crystallography (*10*, *11*), respectively (for sequences of the

[†] The present work was supported by Grant 31-46′998.96 from the Swiss National Science Foundation and by the Fonds der Chemischen Industrie. A.D. and M.H. were supported by a Doktoranden-Stipendium of the Fonds der Chemischen Industrie. H.F. was supported by a fellowship of the DFG (Eg 53/3-3). H.S. and M.M. were supported by and all measurements have been performed at the Large Scale Facility for Biomolecular NMR at the University of Frankfurt (ERB CT 95 00 34) and by the Italian Ministery of University and Scientific Research (MURST-PRIN, 1998).

[‡] The coordinates of the 26 final CaM/C20W structures have been deposited in the Brookhaven Protein Data Bank under the PDB ID code 1CFF. The chemical shift assignment of CaM/C20W has been deposited in the BioMagResBank database, with accession number 4284.

* To whom correspondence should be addressed. C.G.: Institute of Organic Chemistry, University of Frankfurt, Marie-Curie-Strasse 11, D-60439 Frankfurt, Germany. E-mail: cigr@org.chemie.uni-frankfurt.de. Phone: +49 69 79829130. Fax: +49 69 79829128. J.K.: Institute of Biochemistry, Swiss Federal Institute of Technology (ETH), CH-8092 Zurich, Switzerland. E-mail: krebs@bc.biol.ethz.ch. Phone: +41 1 632 3005. Fax: +41 1 632 1591.

[§] Institute of Organic Chemistry, University of Frankfurt, D-60439 Frankfurt, Germany.

[||] Institute of Biochemistry, Swiss Federal Institute of Technology (ETH), CH-8092 Zurich, Switzerland.

[⊥] Current address: BACHEM AG, Hauptstrasse 144, CH-4416 Bubendorf, Switzerland.

[#] Current address: Department of Biochemistry, University of Padova, 35121 Padova, Italy.

10.1021/bi9908235 CCC: $18.00
Published on Web 08/27/1999

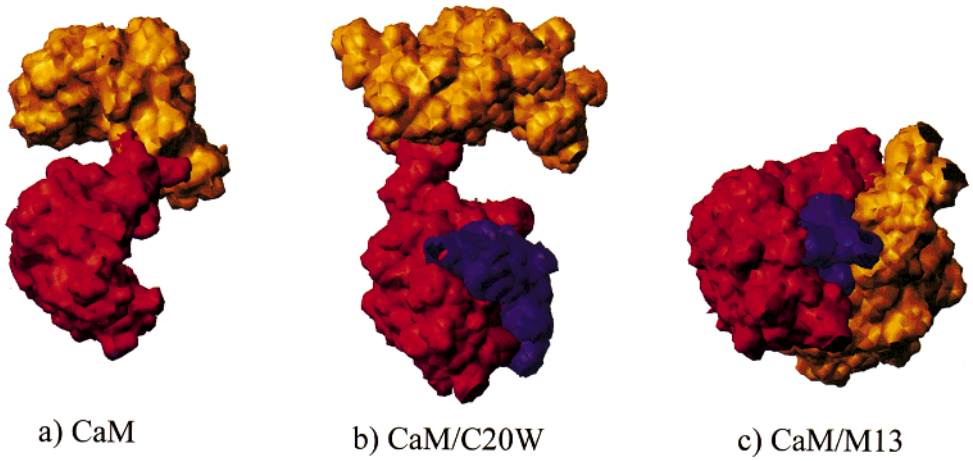

FIGURE 1: Surface representation of $(Ca^{2+})_4$-calmodulin (CaM) and its different binding modes to peptides. The N-terminal half of CaM (residues 1−78) is in orange, the C-terminal half (residues 79−148) is in red, and the peptides are in blue. The orientation of the C-terminal half of CaM is the same in all cases. The structures of $(Ca^{2+})_4$-CaM and of the CaM/M13 complex are based on coordinates taken from the Brookhaven Protein Data Bank [entries 3CLN (*12*) and 2BBM (*9*)]. The CaM/C20W coordinates are from the structure reported here. (a) Surface representation of the crystal structure of $(Ca^{2+})_4$-CaM. The dumbbell shape of CaM comprises two globular domains, each of which contains two Ca^{2+} binding sites and which are connected by a long rigid central helix. In solution NMR studies indicate that the central helix is disrupted near its midpoint and serves as a flexible linker between the two domains (*6*, *7*). (b) Solution structure of the CaM/C20W complex showing that the peptide C20W, corresponding to the N-terminal portion of the CaM-binding domain of the plasma membrane Ca^{2+} pump, binds only to the C-terminal half of CaM. The flexible tether region between the N- and C-terminal domains allows large variations in the orientation of one domain relative to the other. Thus, this depicted structure taken from the ensemble of 26 final structures shows a specific orientation of the two halves. (c) The solution structure of CaM/M13 shows a compact globular complex involving both C- and N-terminal halves of CaM in binding the peptide M13 corresponding to the CaM-binding domain of MLCK.

Table 1: Peptide Sequences from the CaM Binding Domains of CaM Target Proteins[a]

																splice site ↓														
	-6	-5	-4	-3	-2	-1	1	2	3	4	5	6	7	8	9	10	11	12	13	14	15	16	17	18	19	20	21	22	23	24	25	26
C20W			L	R	R	G	Q	I	L	W	F	R	G	L	N	R	I	Q	T	Q	I	K										
C24W							Q	I	L	W	F	R	G	L	N	R	I	Q	T	Q	I	R	V	V	N	A	F	S	S	S		
C28W			L	R	R	G	Q	I	L	W	F	R	G	L	N	R	I	Q	T	Q	I	R	V	V	N	A	F	S	S	S		
skMLCK(M13)							K	R	R	W	K	K	N	F	I	A	V	S	A	A	N	R	F	K	K	I	S	S	S	G	A	L
smMLCK(R20)						A	R	R	K	W	Q	K	T	G	H	A	V	R	A	I	G	R	L	S	S						
CaMKII		L	K	K	F	N	A	R	R	K	L	K	G	A	I	L	T	T	M	L	A	T	R	N	F	S					
CaMKI							A	K	S	K	W	K	Q	A	F	N	A	T	A	V	V	R	H	M							

[a] The alignment of the peptides is based on the first hydrophobic anchor residue shown in dark shading. which interacts with the C-terminal half of CaM. The second anchor residue interacting with the N-terminal half (missing in C20W) is shown in light shading. The numbering of the residues was chosen using the M13 sequence according to ref *9*. The arrow denotes the splice site in the CaM-binding domain (between Q_{14} and I_{15}) due to which different isoforms of the calcium pump may occur, differing in their sequence downstream of the splice site (*24*).

different peptides see Table 1). Several conclusions have emerged from these studies: (1) The binding of target peptides induces a large conformational change of Ca^{2+}-saturated CaM, which bends from the extended shape revealed by crystallographic work (*12*) into a more globular structure in which the two halves of the protein wrap around the target peptide (Figure 1c). In each binding peptide two hydrophobic residues spaced by 8 or 12 positions (see Table 1) are key to the interaction with CaM. The first residue is often a tryptophan (for a review see ref *13*). (2) The CaM-binding peptides, which are mainly random coil in solution, adopt α-helical structures in the complex with CaM, interacting with the latter in an antiparallel manner; i.e., the N-terminal half of CaM binds the C-terminal part of the peptide and vice versa.

The plasma membrane Ca^{2+} pump, a CaM target protein, is one of the key enzymes controlling the Ca^{2+} level in cells. The enzyme is an essential component of all animal plasma membranes and is the product of at least four genes with additional isoforms produced by alternative splicing (*14*). The CaM-binding domain has a length of ca. 30 amino acids, i.e., $AA_{1100-1127}$ of hPMCA1b (*15*), and has the expected propensity to form an amphiphilic helix of basic and apolar amino acids. It functions as an autoinhibitory domain of the pump, binding to two "receptor" sites near the active center (*16*, *17*) of the Ca^{2+} pump. The N-terminal region of the CaM-binding domain interacts with a site located between the phosphorylatable aspartate (D_{475}) and the FITC- (ATP-) binding site (K_{609}), whereas the C-terminal part interacts with

[1] Abbreviations: CaM, calmodulin; C20W, N-terminal portion of the CaM-binding domain of the plasma membrane calcium pump; TR2C, C-terminal tryptic fragment (residues 78−146) of CaM; NMR, nuclear magnetic resonance; MLCK, myosin light chain kinase; CaMKIIα, calmodulin kinase IIα; SAXS, small-angle X-ray scattering; TPPI, time-proportional phase incrementation; ppm, parts per million; DSS, 2,2-dimethyl-2-silapentane-5-sulfonate, sodium salt; NOE, nuclear Overhauser effect; rmsd, root-mean-square deviation; M13, CaM-binding domain of MLCK; smMLCK, smooth muscle MLCK; R20, CaM-binding domain of smMLCK; CaMKI, calmodulin kinase I; ATP, adenosine triphosphate; pH*, uncorrected pH meter reading for D_2O solution.

the cytoplasmic loop between transmembrane domains 2 and 3, corresponding to the "transduction unit" of P-type ATPases (*14*).

Unique among CaM targets, the plasma membrane Ca^{2+} pump can be activated by the C-terminal but not the N-terminal half of CaM (*18*), isolated after trypsin cleavage. In other cases of CaM targets isolated CaM fragments may bind the target without activation (e.g., see refs *19*, *20*), or both fragments, i.e., the N- and the C-terminal halves of CaM (*21*, *22*), are necessary for activation. This raises the question of the mode of CaM interaction with the binding domain of the pump, especially which part of the CaM-binding domain of the Ca^{2+} pump is sufficient to interact solely with the C-terminal half of CaM. We have addressed this problem by dissecting the binding domain in peptide models of various length (the sequences are shown in Table 1). In addition, previous experiments provided evidence that a splicing site was located in the middle of the CaM-binding domain (*23*) which to the best of our knowledge has not been observed for other CaM targets. This has the consequence that only the upstream, N-terminal part of the binding domain is identical in all isoforms (*23*; see Table 1). Thus, it was decided to study the complex between CaM and a shorter peptide C20W, stopping just close to the splice site and short of the putative second CaM anchor residue. The Ca^{2+}-dependent affinity of this peptide for CaM is comparable to the affinity of CaM for the native enzyme (*24*).

Small-angle X-ray scattering studies (SAXS) (*25*) have been previously performed on complexes of CaM with peptides C20W and C24W (*26*) (Table 1), corresponding to different portions of the CaM-binding domain of the plasma membrane Ca^{2+} pump. The results indicate that the complex of CaM with peptide C24W, which contains both anchoring hydrophobic residues, has a globular shape as observed with other CaM-binding peptides. The SAXS data on the complex of CaM with peptide C20W, on the other hand, which lacks the second hydrophobic anchor residue in the peptide, are indicative of flexibility between the two CaM domains (*26*) typical for CaM in solution (*25*).

The solution structure of the CaM/C20W complex described in the present study indeed shows that the peptide is only bound to the C-terminal half of CaM (Figure 1b). Analysis of NMR ^{15}N relaxation data also indicates a higher degree of flexibility in the mid-portion of the central helix of CaM in the complex, comparable to free CaM in solution (*6*).

The focus of the present investigation is to define the binding interactions of C20W with CaM and to derive the overall topology of the complex. The interesting finding here is that the CaM/C20W structure resembles a complex halfway on the folding pathway of fully complexed CaM with, e.g., M13, in which both domains of CaM are bound to the peptide. As CaM interacts with a variety of different target enzymes, the determination of structural differences between different CaM complexes is of great importance for the understanding of molecular recognition and specific signaling pathways.

MATERIALS AND METHODS

Sample Preparation. Uniformly ^{15}N- or $^{15}N/^{13}C$-labeled recombinant *Xenopus laevis* (*27*) CaM (identical to mammalian CaM) was expressed in *Escherichia coli* using the expression vector pTSNco12 (*28*). CaM expression was induced by a temperature shift, cells were harvested and lysed, and CaM was isolated by a modification of the procedure described elsewhere (*18*). C20W with natural isotopic abundance was synthesized and purified as described by Vorherr et al. (*24*) and was complexed to CaM in a 1:1 ratio following the procedure described by Ikura et al. (*29*). NMR samples were prepared as 1.7 mM CaM/C20W solutions in a Shigemi tube (Shigemi Inc., Allison Park, PA) containing 140 mM KCl and 7 mM $CaCl_2$ in H_2O and D_2O, respectively. The pH/pH* values of the samples were 6.5 without consideration of the isotope effect.

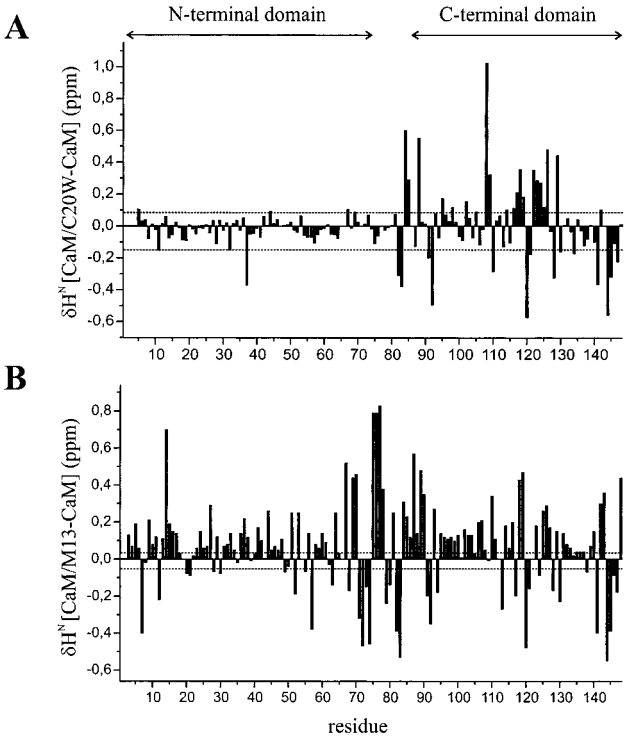

FIGURE 2: Chemical shift differences of the amide protons of (A) CaM/C20W and (B) CaM/M13 (*29*) with respect to Ca^{2+}-loaded CaM (*66*). For the CaM/C20W complex major changes occur only in the C-terminal domain of CaM, suggesting that the peptide C20W binds only to this domain. This is in contrast to the CaM/M13 complex where both domains are involved in binding the peptide M13, and hence chemical shift changes can be observed over the complete amino acid sequence of CaM. It should be noted that the NMR experiments of the three CaM systems were measured at different temperatures: Ca^{2+}-loaded CaM at 320 K (47 °C), CaM/C20W at 303 K (30 °C), and CaM/M13 at 309 K (36 °C). However, the differences between chemical shifts in the three compared systems are larger than the expected temperature-induced chemical shift perturbations (marked as dotted horizontal lines).

For the preparation of the C-terminal tryptic fragment of CaM (TR2C) CaM was isolated from bovine brain as described before (*18*). It was cleaved by trypsin in the presence of Ca^{2+} according to Walsh et al. (*30*) as described elsewhere (*18*). The fragments were purified according to Toda et al. (*31*). The C-terminal fragment (TR2C) comprised residues Asp78−Lys148. An NMR sample was prepared as 2 mM TR2C/C20W solution in 90% H_2O/10% D_2O, 100 mM KCl and 5 mM $CaCl_2$ with pH value of 6.3.

NMR Spectroscopy. All spectra were recorded at a temperature of 303 K using Bruker DRX600 and DRX800 spectrometers equipped with four frequency channels and a

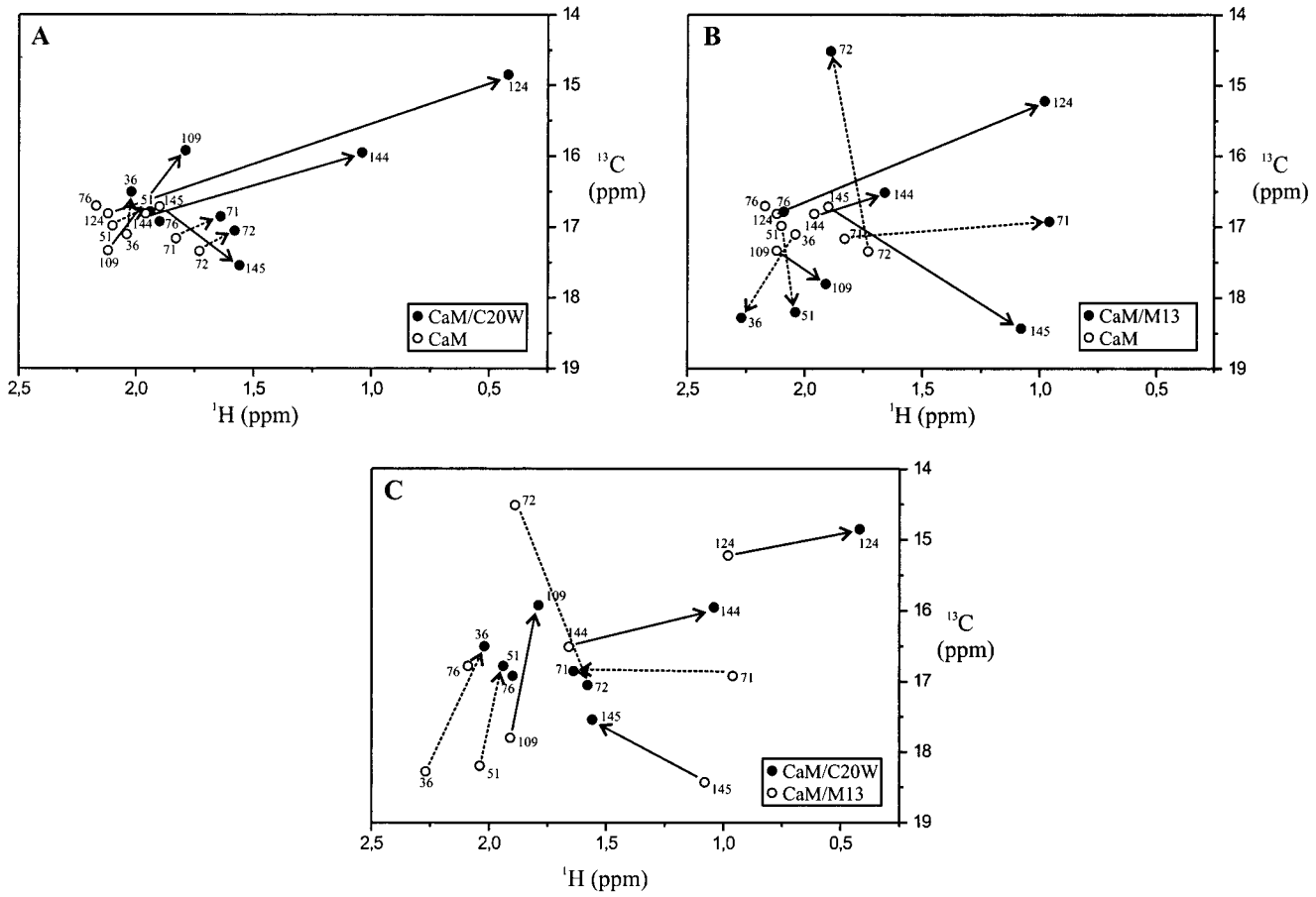

FIGURE 3: Schematic ^{1}H,^{13}C HSQC spectra of the ϵCH$_3$ groups of the methionine residues in CaM (*68*) and the CaM/C20W and CaM/M13 (*68*) complexes. Chemical shift differences of methionines of the C-terminal domain of CaM (Met109, Met124, Met144, Met145) are indicated with solid arrows, and the differences of the methionines of the N-terminal domain of CaM (Met36, Met51, Met71, Met72) are indicated with dotted arrows. Met76 is a residue of the flexible linker region. (A) The comparison between CaM and the CaM/C20W complex shows large chemical shift differences of methionines only of the C-terminal domain of CaM. (B) Upon binding of the peptide M13 to both domains of CaM, methionines of both domains are largely shifted. (C) When the CaM/C20W and CaM/M13 complexes are compared, the methionines of the C-terminal domain show large chemical shifts due to the different side-chain conformations in the two complexes. The methionines of the N-terminal domain in CaM/C20W reveal only small chemical shift dispersion similar to the ones in free Ca^{2+}-saturated CaM whereas in the CaM/M13 complex the corresponding methionines are widely dispersed. In both complexes the resonance of Met76 which is part of the flexible tether region is close to the random coil value.

triple-resonance three-axis gradient probe. All experiments with H^N detection were carried out using pulsed field gradients for coherence-order-selective coherence transfer (*32*−*34*) with minimal water saturation (*35*). Quadrature detection in all indirect ^{13}C dimensions was obtained with States−TPPI phase cycling (*36*). In all experiments a relaxation delay of 1 s was used. All data were processed with UXNMR (Bruker Instruments, Rheinstetten) including zero filling and linear prediction calculations. The spectra were analyzed with FELIX (MSI, San Diego, CA). Proton chemical shifts are reported with respect to the DSS signal (0.0 ppm) at 303 K. The ^{13}C and ^{15}N chemical shifts were indirectly referenced using the following ratios of the zero-point frequencies at 303 K: 0.101329118 for ^{15}N to ^{1}H and 0.251449530 for ^{13}C to ^{1}H (*37*). The sequence assignments for the protein backbone nuclei of the ^{13}C,^{15}N-labeled CaM were mainly achieved by a pair of CBCA(CO)NH and CBCANH (*38*) experiments and further confirmed by another set of experiments, HNCO, HNCA (*38*), HBHA(CO)NH (*39*), HNHA (*40*), and NOESY ^{1}H,^{15}N HSQC (*41*). Side-chain assignments were obtained using HCCH-TOCSY (*42*), (H)CC(CO)NH (*43*), and H(CCCO)NH (*43*). The (HB)CB(CCarom)H experiment using the PLUSH-TACSY (*44*) sequence was recorded to obtain the proton assignments of the aromatic residues of CaM. Methionine methyl groups were assigned via an HMBC HSQC (*45*) and a LRCC experiment (*45*). NOEs within CaM were measured using NOESY ^{1}H,^{13}C HSQC (*46*) and NOESY ^{1}H,^{15}N HSQC (*41*) with mixing times of 150 and 100 ms, respectively. The proton resonances of the peptide C20W which was not labeled could be assigned by a ^{12}C,^{14}N-filtered NOESY experiment with a mixing time of 100 ms. Intermolecular NOEs between CaM and the peptide were measured using a 3D ^{12}C,^{14}N ω_1-filtered NOESY ^{1}H,^{13}C HSQC experiment (*47*) with a mixing time of 150 ms. A HNHA (*40*) experiment was collected in order to obtain $^{3}J_{\mathrm{HNH}\alpha}$ values used to generate qualitative dihedral angle restraints. The experimental $^{3}J_{\mathrm{HNH}\alpha}$ values were multiplied with a correction factor of 1.1 (*48*). For the determination of the $^{3}J_{\mathrm{NC}\gamma}$ and $^{3}J_{\mathrm{C'C}\gamma}$ coupling constants of aromatic side chains of CaM, the experiments ^{15}N-{$^{13}C_{\gamma}^{\mathrm{arom}}$} spin−echo difference ^{1}H,^{15}N HSQC and ^{13}C′-{$^{13}C_{\gamma}^{\mathrm{arom}}$} spin−echo difference ^{1}H,^{15}N HSQC (*49*) were recorded, respectively. Slowly exchanging amide protons were identified by measuring the temperature coefficients of the amide protons from a series of sensitivity-enhanced ^{1}H,^{15}N HSQC spectra recorded at different tem-

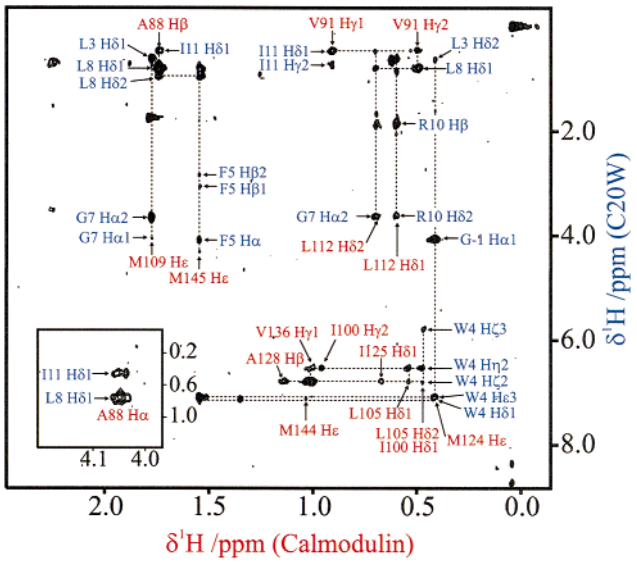

FIGURE 4: 2D ^{1}H,^{1}H projection of the ^{12}C/^{14}N ω_1-filtered 3D NOESY ^{1}H,^{13}C HSQC spectrum containing only intermolecular NOEs between CaM (in red) and the peptide C20W (in blue). Only contacts between the C-terminal half of CaM and the peptide were observed. Assigned cross peaks are indicated in the spectrum.

peratures (301, 303, 305, 307, 309 K). Measurement of ^{1}H/^{2}H exchange rates of the amide protons was hampered by the insolubility of the CaM/C20W complex after lyophilization. ^{15}N relaxation rates and heteronuclear NOE were measured using standard pulse sequences (*50*−*54*) and analyzed according to the model-free Lipari−Szabo approach (*55*, *56*) using the programm MODELFREE 4.0 (*57*, *58*). A list of all recorded NMR experiments with parameters and the ^{1}H, ^{13}C, and ^{15}N resonance assignments are given in Supporting Information. The chemical shifts have also been deposited in the BioMagResBank, with accession number 4284.

Of the unlabeled TR2C/C20W complex a 2D NOESY spectrum with a mixing time of 200 ms was recorded at 303 K using a Bruker AM600 (Spectrospin AG, Fällanden) spectrometer.

Structure Calculations. Distance restraints were classified on the basis of peak intensity with upper bounds of 2.9 Å (strong), 4.2 Å (medium), and 5.7 Å (weak). A correction of 0.5 Å was added to the upper bounds of restraints involving pseudoatoms for methyl groups (*59*). For the lower bounds of the distance restraints the sum of the van der Waals radii was used. The intermolecular restraints were treated in the same way as the intramolecular ones. In the early stage of structure calculation the $^{3}J_{\mathrm{HNH}\alpha}$ coupling constants were used to derive ϕ dihedral angle restraints. For regions with distinct secondary structure identified in the first generation of structures in agreement with characteristic NOE patterns and chemical shift indices (*60*), both ϕ and ψ dihedral angle restraints were included in the final calculations. For α-helical regions ($^{3}J_{\mathrm{HNH}\alpha}$ < 5.5 Hz) dihedral angle values of $\phi = -65°$ (±25°) and $\psi = -40°$ (±25°) were used. For β-strands ($^{3}J_{\mathrm{HNH}\alpha}$ > 8 Hz) the values were taken as $\phi = -120°$ (±30°) and $\psi = 120°$ (±30°) (*61*). From the determined $^{3}J_{\mathrm{NC}\gamma}$ and $^{3}J_{\mathrm{C'C}\gamma}$ values five dihedral angle restraints for aromatic residues were taken as $\chi_1 = 180°$ (±30°) and as $\chi_1 = -60°$ (±30°). Backbone hydrogen bonds were included as pairs of restraints between NH and N atoms to the corresponding carbonyl O atom only when the temperature coefficient of the amide proton of the residue was less than −0.003 ppm/K (*61*, *62*) and the NOE pattern indicated unambiguous donor−acceptor pairs. A total of 61 hydrogen bonds were identified and used as restraints for $r_{\mathrm{NH-O}}$ of an upper bound of 2.4 Å and $r_{\mathrm{N-O}}$ of 3.3 Å in the final stage of the structure determination. In addition, 24 distance restraints between the four Ca^{2+} ions and protein groups derived from the crystal structure of Ca^{2+}-loaded CaM (*12*) were used in the structure calculation. This procedure is similar to published NMR-derived structure determinations of the CaM/M13 complex (*9*) and the CaM/W7 (*63*) complex.

Table 2: Structural Statistics for the CaM/C20W Complex[a]

rmsd from idealized covalent geometry	
bond length (Å)	0.0027 ± 0.0001
bond angle (deg)	0.483 ± 0.009
impropers (deg)	10.3 ± 1.2
rmsd from experimental restraints	
distances (Å)	0.031 ± 0.001
dihedral angles (deg)	0.67 ± 0.11
energies (kcal mol^{-1})	
E_{total}	381 ± 17
E_{bond}	20 ± 2
E_{angle}	170 ± 6
$E_{\mathrm{impropers}}$	29 ± 2
E_{vdW}	63 ± 6
E_{NOE}	96 ± 9
E_{CDIH}	4 ± 1
coordinate precision[b] (Å)	
N-terminal half of CaM (residues L_4−A_{73})	
rmsd of backbone atoms	0.75
rmsd of all heavy atoms	1.17
superposition over secondary structure elements (7−18, 26−38, 47−54, 62−74)	
rmsd of backbone atoms	0.56
rmsd of all heavy atoms	1.08
C-terminal half of CaM (residues I_{85}−T_{145}) and C20W (residues G_{-1}−Q_{12})	
rmsd of backbone atoms	0.53
rmsd of all heavy atoms	1.06
superposition over secondary elements [85−92, 99−112, 118−128, 135−145; C20W (−1)−12]	
rmsd of backbone atoms	0.50
rmsd of all heavy atoms	1.07

[a] Refers to the ensemble of the final 26 structures with lowest energy. [b] Rmsd between the ensemble of 26 structures and the mean structure.

For all calculations the X-PLOR program, version 3.851, by Brünger (*64*) was used. The ab initio simulated annealing protocol started with a 32.5 ps high-temperature phase at 2000 K, followed by a first cooling phase of 25 ps, where the temperature was lowered to 1000 K in steps of 50 K. In the second cooling phase the temperature was lowered to 100 K, followed by a final energy minimization. A total of 1857 NOE-derived distance restraints were applied with a square-well potential and a force constant of 50 kcal·mol^{-1}·Å^{-2}. Restraints involving methylene protons which were not stereospecifically assigned were treated with the floating assignment procedure of X-PLOR. A total of 129 dihedral angle restraints from $^{3}J_{\mathrm{HNH}\alpha}$, $^{3}J_{\mathrm{NC}\gamma}$, and $^{3}J_{\mathrm{C'C}\gamma}$ coupling constant measurements were also applied with a force constant of 200 kcal·mol^{-1}·rad^{-2}. The final 26 structures with the lowest energy were used for the structural statistics (Table 2). This ensemble of 26 structures satisfied the criteria of no NOE violation >0.5 Å and no dihedral violations >5°. The coordinates have been deposited with the Protein Data Bank, Chemistry Department, Brookhaven National Laboratory, with accession code 1CFF. All structure displays in

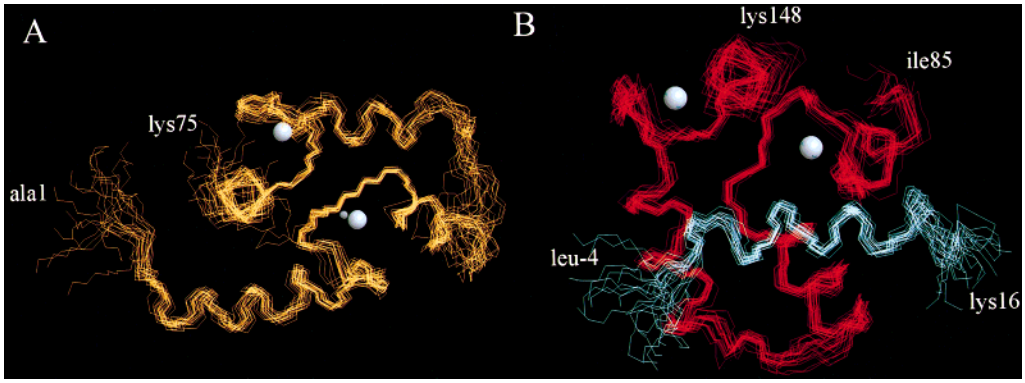

FIGURE 5: Best-fit superpositions of the backbone atoms (N, Cα and C′) of (A) the N-terminal domain (in orange) and (B) the C-terminal domain (in red) of the final 26 NMR-derived structures of the CaM/C20W complex. The peptide C20W (in blue) binds only to the C-terminal half of CaM. The residues of the N- and C-termini of each domain and of the peptide are indicated, and the Ca^{2+} ions are shown as gray balls. For the N-terminal domain (residues 4−73) superposition yields a rmsd value of 0.85 Å for all backbone atoms and 1.27 Å for all heavy atoms referring to a mean structure. For the backbone and all heavy atoms of the C-terminal domain (residues 85−145) together with the peptide C20W [residues (−1)−12] the rms deviations are 0.57 and 1.08 Å, respectively.

the figures were created using the program MOLMOL by Konradi et al. (*65*).

RESULTS AND DISCUSSION

NMR Spectroscopy of the CaM/C20W Complex. The structure of the complex between Ca^{2+}-saturated, ^{13}C,^{15}N-labeled CaM and nonlabeled peptide C20W (corresponding to the N-terminal portion of the CaM-binding domain of the plasma membrane Ca^{2+} pump) was determined by multidimensional, heteronuclear NMR spectroscopy. A set of heteronuclear three-dimensional experiments yielded the assignment of 95% of the backbone atoms (H^N, N, C^α, C′) of CaM, of most of its side chains, and 74% of the peptide proton resonances (the assignment is given in Supporting Information). The assignment of the protein part of the CaM/C20W complex was especially difficult for the N- and C-terminal residues and the flexible linker region (residues Arg74 to Glu84) where cross-peaks were found to be broad and weak presumably due to the slow conformational flexibility in these regions. The unlabeled peptide part was assigned from a ^{12}C,^{14}N-filtered NOESY experiment. Figure 2A shows the difference of the amide proton chemical shift of the CaM/C20W complex to the shifts of Ca^{2+}-loaded CaM (*66*). The most notable changes are seen in the C-terminal domain of CaM, whereas almost no changes occur in the N-terminal domain. This result suggests that the peptide C20W binds only to the C-terminal domain but not to the N-terminal domain of CaM. In contrast, the amide proton chemical shift difference between the CaM/M13 complex (*29*) and Ca^{2+}-loaded CaM (*65*) shown in Figure 2B is clearly indicative of M13 binding to both domains of CaM. Despite the fact that the NMR experiments of the three CaM systems were measured at different temperatures, Ca^{2+}-loaded CaM at 320 K (47 °C), CaM/C20W at 303 K (30 °C), and CaM/M13 at 309 K (36 °C), the differences between chemical shifts in the three compared systems are larger than the expected temperature-induced chemical shift perturbations for the complexes studied as marked in Figure 2 as dotted horizontal lines.

For the structure determination of the complex the assignment of the ϵCH_3 groups of the nine methionine residues of CaM was crucial, because methionines are mainly involved in binding the target peptides of CaM (*67*). The 3D HMBC HSQC experiment correlating the $^1H\epsilon$ and the $^{13}C\epsilon$ chemical shifts over the sulfur atom with the $^{13}C\gamma$ chemical shift together with information from NOESY spectra allowed the assignment of all nine methionine methyl groups. Met124 and Met144, which are both involved in the binding of the tryptophan residue of the C20W peptide, exhibit a large upfield shift due to ring current effects of the Trp aromatic ring. In Figure 3A the chemical shifts of the ϵCH_3 groups of the methionines in CaM (*68*) and in the CaM/C20W complex are compared in a schematic ^1H,^{13}C HSQC spectrum. All methionines of the C-terminal half (Met109, Met124, Met144, Met145) of CaM show a large chemical shift upon complexation with the peptide C20W (solid arrows), whereas all methionines of the N-terminal half (Met36, Met51, Met71, Met72) have similar shifts in free CaM and in the CaM/C20W complex (dotted arrows). This observation provides additional evidence that the peptide binds only to the C-terminal domain of CaM but not to the N-terminal domain. In the CaM/M13 complex the methionines of both domains show large chemical shift deviations when compared to the methionines in CaM (Figure 3B) due to the fact that both domains of CaM are involved in binding of the peptide M13. The importance of methionines in CaM molecular recognition will be discussed in the section Comparison of the CaM/C20W Complex with Other CaM/Peptide Complexes.

The 3D ^{13}C- and ^{15}N-separated NOESY experiments were used to identify 1645 NOE restraints (794 intraresidual, 387 sequential, 311 medium range, and 153 long range) within CaM, corresponding to an average of 15.6 NOEs per residue (*69*). A figure showing the number of NOE restraints per residue is given in Supporting Information. For peptide C20W, 163 intramolecular NOE restraints (102 intraresidual, 32 sequential, 29 medium range) could be assigned from the ^{12}C,^{14}N-filtered NOESY experiment, suppressing the signal of ^{13}C- and ^{15}N-attached protons. A total of 49 intermolecular NOEs between the peptide and the protein, detected in the 3D ^{12}C,^{14}N ω_1-filtered NOESY ^1H,^{13}C HSQC experiment, defined the interface between the two molecules. The 2D ^1H,^1H skyline projection of this 3D experiment is depicted in Figure 4. For example, the side chain of the single tryptophan residue of C20W at position 4 shows numerous NOE interactions to the methyl groups of Ile100, Leu105,

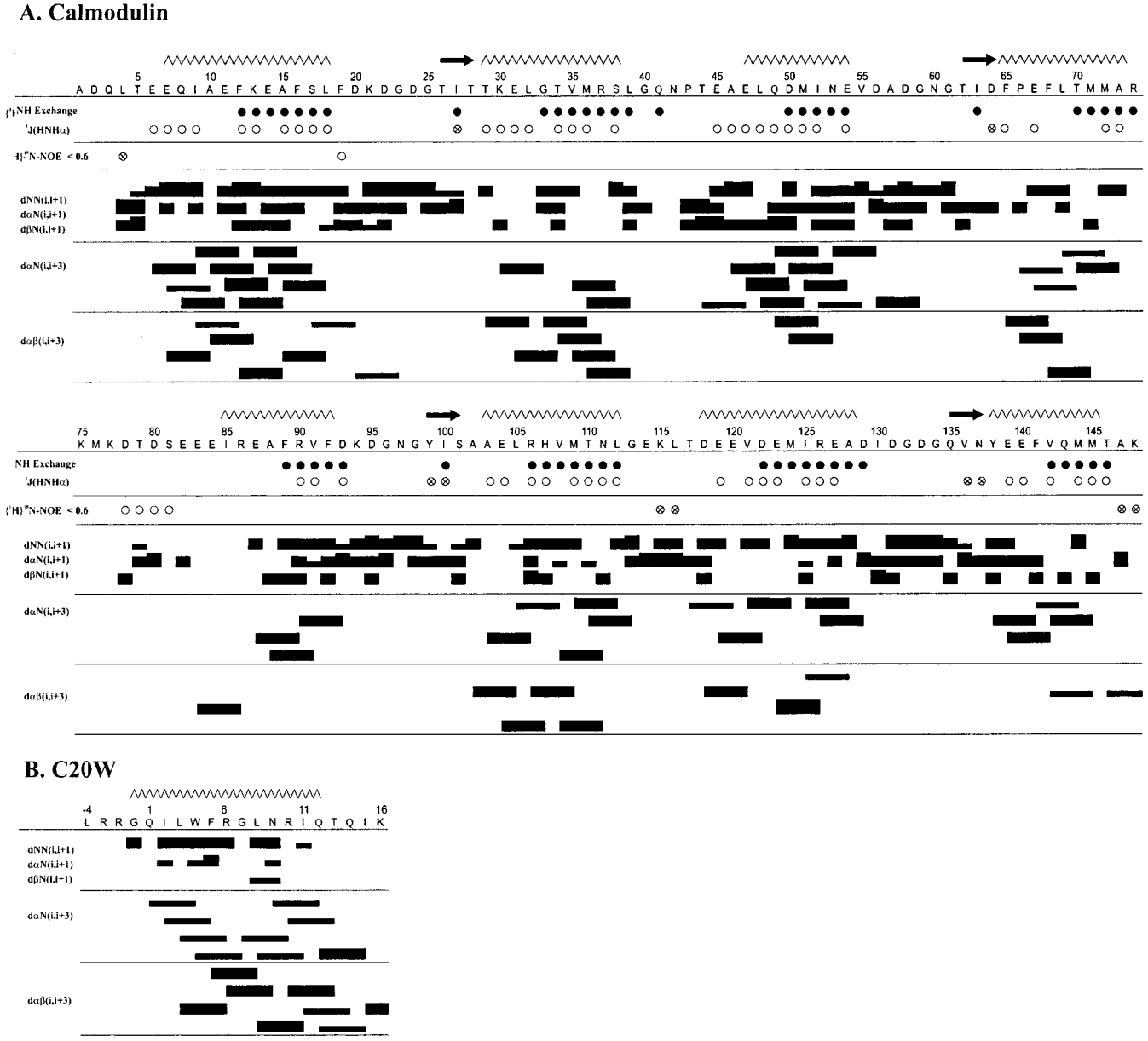

FIGURE 6: Summary of sequential and medium-range NOEs involving HN, CαH, and CβH protons, slowly exchanging amide protons, $^3J_{HNH\alpha}$, and {^{1}H}^{15}N heteronuclear NOE values for the CaM/C20W complex. The amino acid sequence and residue numbers together with the secondary structure elements (zigzag line for α-helix, arrows for β-sheet) are shown at the top of the figure. Slowly exchanging amide protons of CaM represented as full circles were identified by measuring the temperature coefficients from a series of ^{1}H,^{15}N HSQC spectra recorded at different temperatures (301, 303, 305, 307, 309 K). Small (<5.5 Hz) and large (>8 Hz) values of $^3J_{HNH\alpha}$ are represented by open circles and crossed circles, respectively. {^{1}H}^{15}N heteronuclear NOE values between 0.6 and 0.4 are depicted by open circles and {^{1}H}^{15}N heteronuclear NOE values less than 0.4 by crossed circles. Sequential and medium-range NOEs classified as strong, medium, and weak according to the intensity of the cross-peak are indicated by different heights of the connecting box.

Met124, Ile125, Ala128, Val136, and Met144 of CaM. In the final stage of the structure calculation 52 intramolecular hydrogen bond restraints were incorporated for CaM, on the basis of the temperature dependence of amide proton chemical shifts (*61*, *62*), and 9 for the peptide C20W. The acceptor of the hydrogen bond was identified with structures calculated only from NOE restraints. In addition, 24 distance restraints between the four Ca^{2+} ions and atoms of the protein derived from the crystal structure of Ca^{2+}-loaded CaM (*12*) were used in the structure calculation.

Structure of the CaM/C20W Complex. The listed structural restraints were used in a simulated annealing protocol (*70*) using X-PLOR (*64*) (for details see Materials and Methods) to calculate a final set of 26 structures. Due to the lack of NOEs between the N- and C-terminal domain, it is impossible to superimpose both domains simultaneously, and therefore the structure of the two domains is presented separately. Figure 5 illustrates a best-fit superposition of the backbone atoms of the N-terminal domain (panel A) and of the C-terminal domain with the bound C20W peptide (panel B). The amino (residues 1−3) and the carboxyl (residues 146−148) termini of CaM, the tether connecting the two domains of CaM (residues 74−84), and the amino (residues −4 to −2) and the carboxyl (residues 13−16) termini of C20W are ill-defined by the NMR data and appear disordered. The final 26 structures are converged with an rmsd from the mean structure of 0.75 Å for all backbone atoms in the N-terminal domain of CaM (residues 4−73) and 0.53

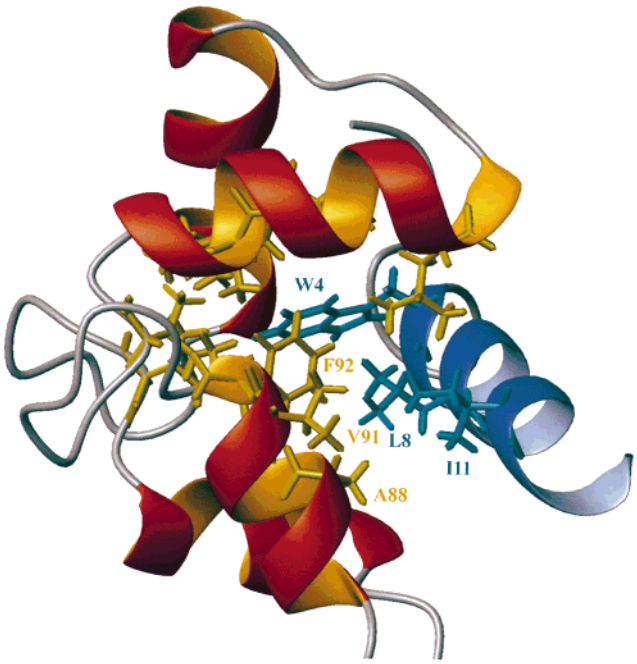

FIGURE 7: Ribbon representation of the C-terminal half of CaM (in red) complexed to the peptide C20W (in blue). The binding of the peptide is stabilized by hydrophobic contacts between W_4, L_8, and I_{11} of the peptide and side chains of CaM. Selected residues involved in the binding are shown. The interaction between the aromatic systems of peptide W_4 and CaM F_{92} giving rise to the large chemical shift perturbation (see Figure 10) is also shown.

Å for all backbone atoms in the C-terminal domain of CaM (residues 85−145) and the peptide C20W [residues (−1)−12] and with low rmsds from the experimental restraints and idealized covalent geometry. The 26 structures exhibited no distance violations exceeding 0.5 Å or dihedral angle violations exceeding 5° and have on average 73.7% of all residues in the most favorable region of the Ramachandran plot according to the PROCHECK (*69*) procedure. Only 1.5% of all residues are found in disallowed regions of the Ramachandran plot. The structural statistics are summarized in Table 2.

The structure of the CaM/C20W complex contains the following secondary structure elements within CaM: Eight α-helix segments identified from the NMR data (Figure 6A) are located at Glu7 to Leu18, Thr29 to Ser38, Glu47 to Glu54, Phe65 to Ala73, Ile85 to Phe92, Ala103 to Leu112, Asp118 to Ala128, and Tyr138 to Met145. Two short antiparallel *β*-sheets connect the strands Thr26 to Thr28 and Thr62 to Asp64 and the strands Tyr99 to Ser101 and Gln135 to Asn137, respectively. Compared to Ca^{2+}-CaM the backbone conformation and the secondary structure remain essentially unchanged upon complexation with the peptide C20W. A superposition of the CaM/C20W complex with Ca^{2+}-CaM reveals a rmsd value of 1.57 Å for the backbone atoms over the N-terminal domain (residues 7−73) and 1.56 Å over the C-terminal domain (residues 85−145). In the structures of other CaM/peptide complexes (*9*−*11*) and of complexes of CaM with small organic compounds (*63*), the backbone conformation of CaM is also highly conserved upon complexation. The peptide C20W, which has a random coil structure in solution, adopts an α-helical structure upon complexation with the C-terminal domain of CaM. The helix extends from residue Gly(−1) to Gln12 (Figure 6B; for nomenclature see Table 1) and shows amphiphatic properties. The hydrophobic side of the helix (Trp4, Leu8, Ile11) is bound to the C-terminal domain of CaM, which the complex CaM/C20W stabilizes by numerous hydrophobic interactions. The hydrophilic side of the helical peptide which contains several basic amino acids [Arg(−3), Arg6, Arg10) is accessible to the surrounding water molecules.

There are no NOE interactions between the N-terminal and the C-terminal domains of CaM, indicating that the two domains do not interact directly on a time scale where NOE interactions can be observed. A flexible tether region extending from Arg74 to Glu84 connects the two domains, and therefore large variations in the orientation of one domain relative to the other occur randomly in the 26 final structures. For the tether region no NMR evidence for α-helical structure like medium-range NOEs was found (Figure 6A). The dynamics of the tether region of Ca^{2+}-loaded CaM in solution indicated flexibility by NOE data, backbone amide hydrogen exchange studies (*7*), and ^{15}N NMR relaxation measurements (*6*). Flexibility of this region can also be concluded for the CaM/C20W complex from the decreased values of the $\{^1H\}^{15}N$ heteronuclear NOE (Figure 6A). Comparison of the absolute values of the heteronuclear NOE is difficult because the investigations have been carried out under different experimental conditions. The heteronuclear NOE data, however, indicate that the flexibility of CaM/C20W is decreased compared to CaM without target peptide, because different from the free CaM, the values of the heteronuclear NOE for the central helix are larger than for the residues Lys115−Leu116 within the loop region G_{113}−T_{117} in the C-terminal domain of CaM.

Comparison of the CaM/C20W Complex with Other CaM/Peptide Complexes. The most striking difference was noticed in the global structure of the CaM/C20W complex as compared to the complex of CaM with M13, the CaM-binding peptide of MLCK (*9*). Only the C-terminal half of CaM binds to the peptide, with no detectable contacts between the peptide and the N-terminal half of CaM. As a result, and different from the structures determined previously, the extended structure of CaM appears to be retained in the complex (Figure 1). Local structural differences in the CaM/C20W complex, as compared to the CaM/M13 complex, are also detected. The C20W peptide adopts an α-helical structure from G_{-1} to Q_{12}, which extends the helix by one turn toward the N-terminus and reduces it by two turns toward the C-terminus with respect to the helical structure of M13 from W_4 to S_{21}. The peptide C20W interacts with CaM via three hydrophobic amino acids (W_4, L_8, and I_{11}) (Figure 7), corresponding to W_4, F_8, and V_{11} in the M13 peptide. However, in the CaM/M13 complex only W_4 interacts with M124 in CaM, whereas in peptide C20W additional contacts with M_{124} are made by the residues G_{-1} and L_3. However, in R20 (*10*), a peptide derived from smMLCK, and also in another peptide derived from CaMKII (*11*), a contact between M_{124} and A_{-1} (corresponding to G_{-1} in peptide C20W) has been observed. In both cases, the additional N-terminal helical turn observed in peptide C20W is also present. A further difference concerns F_{92}, which has NOE contacts only to W_4 in peptide C20W, whereas it interacts with W_4, N_7, F_8, and V_{11} in peptide M13. Apparently, the position of V_{11} in M13 is critical, since it interacts with both CaM halves (*9*, *13*), whereas the corresponding

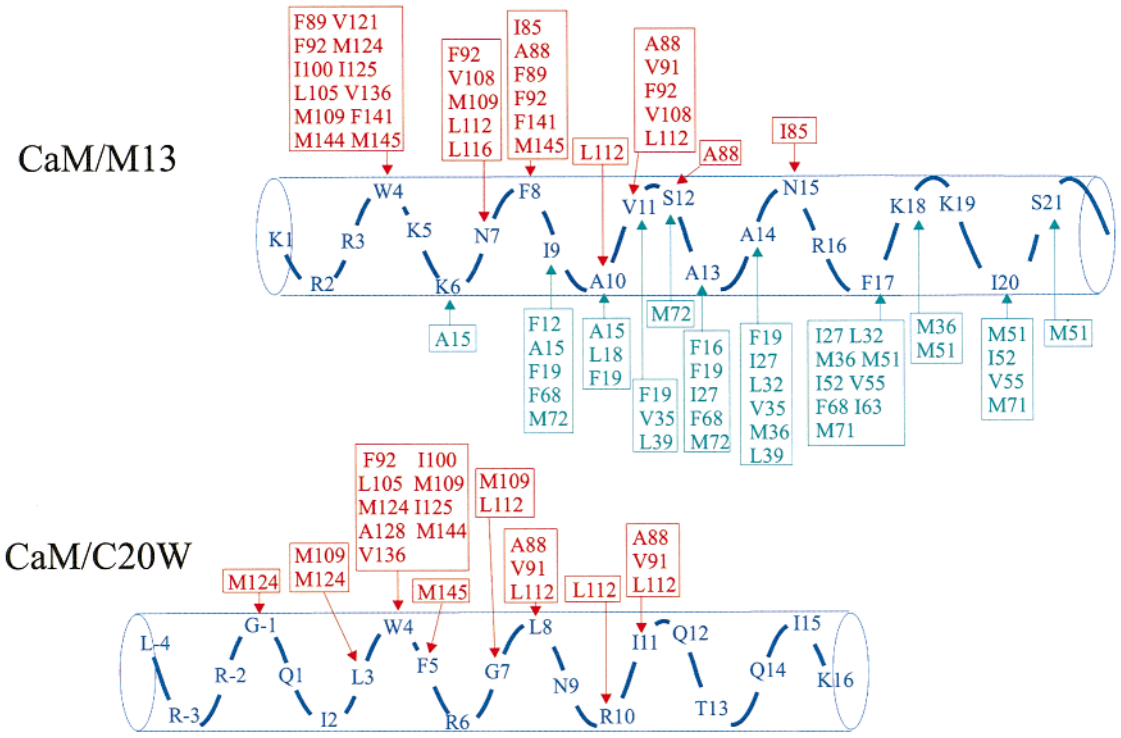

FIGURE 8: Schematic representation of residue pairs for which intermolecular NOEs between CaM and the peptides C20W and M13 are observed.

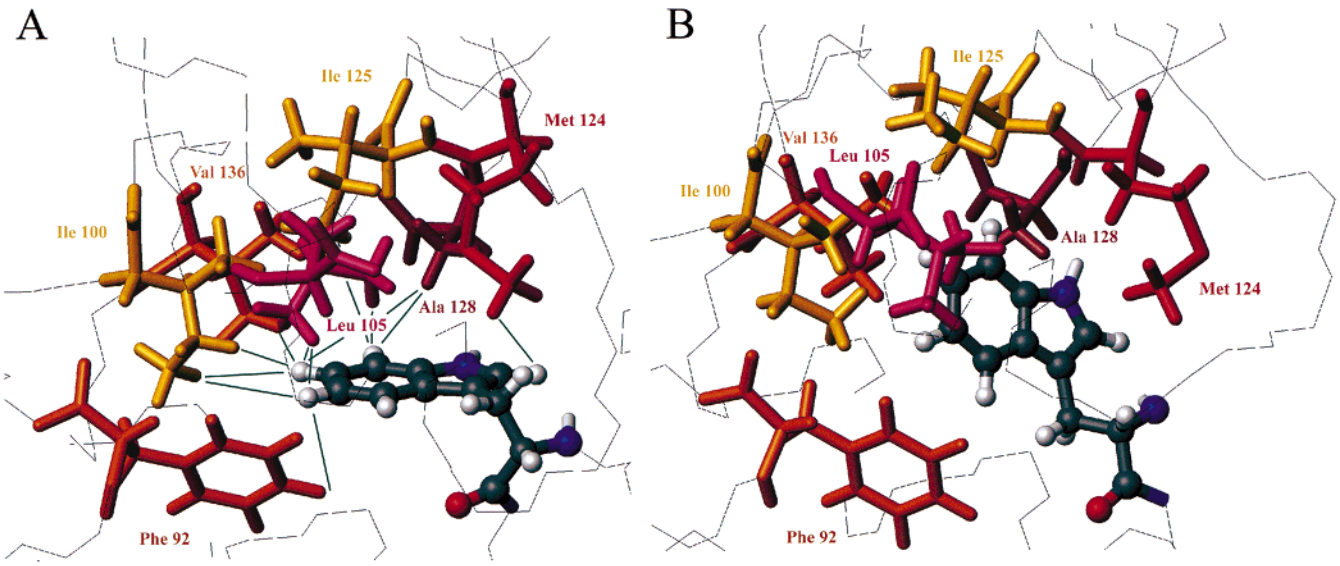

FIGURE 9: Comparison of tryptophan environments in the CaM/C20W (A) and CaM/M13 (B) complexes. The backbones of the C-terminal halves (residues 85−145) of CaM were superimposed (rmsd = 1.47 Å). Experimental NOEs observed between W_4 and the residues of CaM are shown as green lines for CaM/C20W. The plane of the indole ring of W_4 in CaM/C20W is rotated by almost 90° with respect to the one in CaM/M13. In the case of CaM/C20W the C−Hζ3 proton is pointing toward the center of the aromatic ring of F_{92} leading to a strong upfield shift of −1.30 ppm for this proton (see Figure 10). For CaM/M13 F_{92} is further away and the plane normal does not point toward C−Hζ3.

I_{11} in peptide C20W only interacts with residues in the C-terminal half of CaM (A_{88}, V_{91}, L_{112}). Interestingly, A_{10}, the other M13 residue which makes major contacts to both halves of CaM (*13*), is replaced by an arginine residue in C20W, for which no contacts are observed in the CaM/C20W complex. A summary of the contacts between CaM and the peptides C20W and M13, respectively, is presented in Figure 8.

An interesting observation, however, is made concerning the topological orientation of W_4: In peptide C20W the orientation of the indole ring is turned about 90° with respect to M13 (Figure 9). Possibly, the absence of interactions between peptide C20W and the N-terminal half of CaM is responsible for this topological difference. This suggestion is supported by the very similar chemical shift values of the indole ring protons observed in a complex between peptide C20W and the C-terminal tryptic fragment of CaM (TR2C, residues 78−148). In addition, calculations of secondary chemical shifts by the method of Case (*71*) using the program MOLMOL (*65*) yields the values given in parentheses in Figure 10. Only contributions of ring currents of neighboring phenyl groups are considered. These values are in good

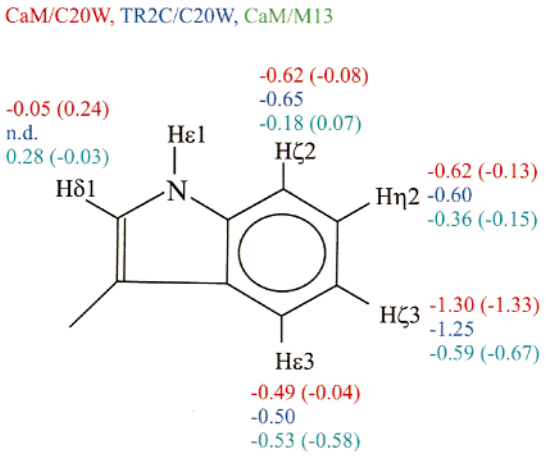

FIGURE 10: Experimental secondary chemical shifts of the tryptophan indole protons of the CaM-bound peptides in CaM/C20W, TR_2C/C20W and CaM/M13. The Hζ3 proton exhibits an extreme upfield shift in the case of CaM/C20W and TR2C/C20W and a much smaller one in the case of the CaM/M13 complex. Calculated values (*70*) are shown in parentheses for CaM/C20W and CaM/M13.

agreement with the experimental data: The largest contribution of the extreme shift of the Hζ3 proton arises from the F_{92} residue in CaM, whereas the contribution of F_5 in peptide C20W (a lysine in M13) is negligible. This is consistent with the difference in orientation of the tryptophan indole rings in the CaM/C20W and CaM/M13 complexes. As opposed to the CaM/M13 complex, the C−Hζ3 bond is directed toward the center of the aromatic ring of F92 in the CaM/C20W complex (Figure 9). Furthermore, aliphatic protons of CaM residues in spatial proximity to the tryptophan exhibit ring current shifts caused by the tryptophan indole ring which could be confirmed by chemical shift calculations.

The ability of CaM to bind to a wide variety of target peptides, which can differ significantly in their amino acid sequences, appears to be related to the high abundance of methionine residues within CaM as discussed in detail by Osawa et al. (*63*). The fine adjustment of side-chain conformations of eight out of nine methionine residues can provide optimized interactions with the target peptides. The methionine side chains are very flexible due to an unbranched side chain and a long C−S bond, which enables essentially free rotation about the χ_3 torsion angle. In addition, sulfur has a larger polarizability than carbon, causing stronger van der Waals interactions (*72*). A comparison of the conformations of the methionines in the binding pocket of the C-terminal domain of CaM (Met109, Met124, Met144, Met145) reveals large differences between the CaM/C20W and CaM/M13 complexes. The ϵCH_3 group of Met109, which is located above the plane of the aromatic ring of the tryptophan in the CaM/M13 complex, is found close to the α- and β-protons of Trp4 in CaM/C20W with only a small conformational change of the side chain. The side-chain conformations of Met144 and Met145 show large changes, but in both complexes the ϵCH_3 groups are in close proximity to the Trp4 aromatic ring. Only the side chain of Met124 shows the same conformation in both complexes with the ϵCH_3 group in contact with the aromatic ring of the tryptophan. The importance of the interaction between Met124 of CaM and the Trp residue in the binding domain of CaMKI (Trp303) for the activation of this kinase has been recently suggested by Chin et al. (*73*) on the basis of the point mutation M124Q which led to a 60-fold increase of the activation constant of CaM. Similarly, previous oxidation experiments of methionine residues provided evidence that Met124 is also important for the activation of the Ca^{2+} pump by CaM (*74*). The described conformational differences are in agreement with the observation that the four Met residues of the binding pocket of the C-terminal domain reveal large chemical shift differences between the two complexes (Figure 3C). Since the N-terminal domain is not involved in the binding of the peptide, the ϵCH_3 groups of the Met residues of the N-terminal domain (Met36, Met51, Met71, Met72) show chemical shifts in the CaM/C20W complex comparable to those in free Ca^{2+}-saturated CaM (Figure 3A). In contrast, in the CaM/M13 complex the resonances are well dispersed due to the binding of the N-terminal methionines to the M13 peptide (Figure 3B,C).

In the structure of the CaM/R20 complex residue Glu84 forms a salt bridge to Arg16 in peptide R20 (*10*). A similar salt bridge to Arg16 may also occur in the CaM/M13 complex and to Lys16 in the CaM/C20W complex studied here: The existence of the salt bridge in the CaM/M13 complex causes chemical shift changes of −0.39/−0.53/−0.31 ppm for the amide protons of the residues Glu82, Glu83, and Glu84 compared to those of free Ca^{2+}-CaM. Similar pronounced chemical shift changes (−0.31/−0.38/0.60 ppm) observed for residues Glu82, Glu83, and Glu84 in CaM/C20W suggest the presence of an equivalent environment. Therefore, similar contacts may exist between K_{16} of peptide C20W and CaM even though these residues are in a region of CaM not defined by long-range NOEs.

Calculation of SAXS data based on the presented structure qualitatively reproduces the experimental finding as documented previously (*26*). However, quantitatively, the compaction indicated in the experimental SAXS data is not reproduced, even if the salt bridge (Lys16/Glu84) is taken into account. Modeling (*55*−*58*) the heteronuclear relaxation data (T_1, T_2, and heteronuclear NOE) to individual correlation times τ_c for both domains leads to comparable values (3% difference) for the two domains in CaM/C20W ($\tau_c^{N-terminal} = 9.8$ ns; $\tau_c^{C-terminal} = 10.1$ ns). This is different from free Ca^{2+}-CaM for which a 12% difference in correlation times for the two domains has been reported (*6*). This is consistent with the SAXS data that show an increased compaction of the CaM/C20W complex as compared to free Ca^{2+}-CaM.

Biological Implications of the Structural Results. The structure described here may help to understand why the Ca^{2+} pump is activated by the isolated C-terminal (and not by the N-terminal) half of CaM. This, together with the significantly higher affinity of peptide C20W for the C-terminal than for the N-terminal half of CaM (*75*), very likely reflects the finding that only the C-terminal half of CaM interacts with the peptide C20W. This peculiar aspect of the interaction may be due to (1) the lack of the second hydrophobic anchor residue at position 17 and (2) the crucial positions of M13 residues A_{10} and V_{11} which interact with both halves of CaM in the CaM/M13 complex (*13*). In the CaM/C20W complex residue I_{11}, equivalent to V_{11} in M13, interacts instead only with the C-terminal half of CaM. Residue R_{10} of C20W (which replaces A_{10} of M13) shows no contacts.

Since most CaM targets are not activated by the two separate halves of CaM (*18*, *19*), it is generally concluded

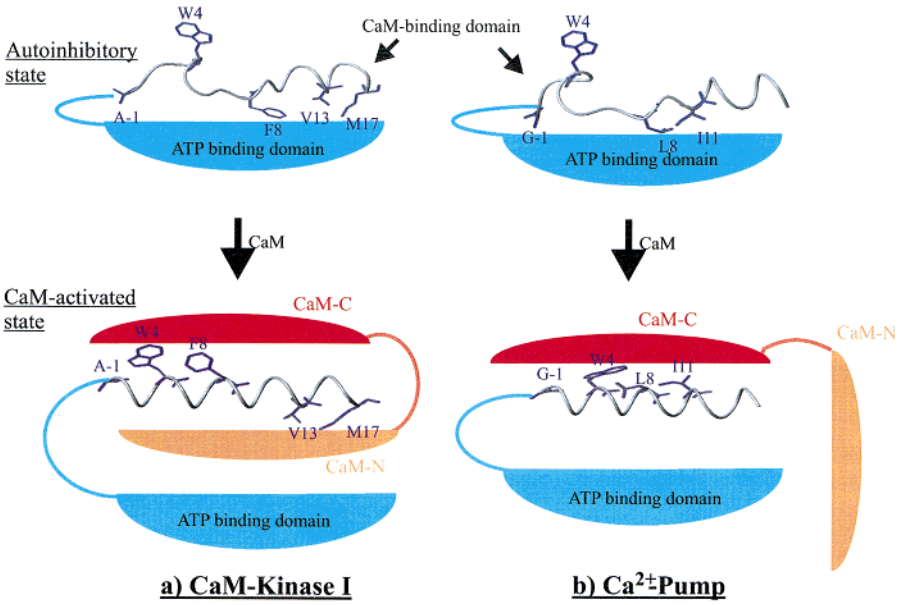

FIGURE 11: Schematic representation illustrating the activation of CaMKI (a) and of the Ca^{2+} pump (b) upon binding of CaM. (a) In the absence of CaM, the CaM-binding domain is bound to the ATP-binding domain of CaMKI, resulting in an autoinhibited state (top). In the crystal structure obtained for this state (*76*) the tryptophan anchor residue is directed outward, suggesting that the initial interaction of the C-terminal half of CaM takes place at this residue. The CaM-binding domain could then undergo a major structural change, adopting α-helical structure, exposing the other hydrophobic residues F_8, V_{13}, and M_{17} to interact with the two halves of CaM, and thereby releasing the ATP-binding domain (bottom). (b) As explained in the text a similar structural model is proposed for the autoinhibited state of the Ca^{2+} pump (top) on the basis of the structure of the CaM/C20W complex and the finding that the pump can be activated by the isolated C-terminal half of CaM. After the initial interaction of the C-terminal half of CaM with W_4 the hydrophobic residues L_8 and I_{11} are displaced from the region next to the catalytic site of the Ca^{2+} pump, thereby releasing the autoinhibited state (bottom). The region of the pump interacting with the CaM-binding domain is defined in the figure as the ATP-binding domain, but it corresponds in fact to the region between the phosphorylated aspartate (D_{475}) and the lysine (K_{609}), which is a component of the ATP-binding domain.

that efficient activation requires the wrapping of CaM around the binding domain and its locking in position by the two hydrophobic anchoring residues mentioned above. In the structure presented here CaM occupies instead only one half-side of the peptide, indicating that activation, i.e., the displacement of the autoinhibitory peptide from its binding site in the pump, is possible without wrapping CaM around it. Thus, it may be proposed (Figure 11) that in the binding of the autoinhibitory peptide to the pump (Figure 11b) residues L_8 and I_{11} [corresponding to L_{1111} and I_{1114} in the pump (*15*)], but not W_4, would establish hydrophobic contacts to the pump to become displaced by the incoming CaM. Figure 11b shows W_4 exposed to the solvent, in analogy to its recently established topology in CaMKI in the absence of CaM (*76*) (see Figure 11a). The importance of W_4 for the interaction with CaM is underlined by the finding that replacing W_4 by an alanine residue reduces the affinity of the peptide for CaM by more than 1 order of magnitude (*24*). The hydrophobic amino acids located in the stretch Phe8−Met17 of the CaMKI peptide are expected to bind to CaM, but they also interact with hydrophobic residues of the ATP-binding domain (*76*) in the kinase. In this context it is of interest that the ATP-binding domain in CaMKI (*76*) contains a hydrophobic sequence similar to the stretch next to the catalytic region of the Ca^{2+} pump (*16*) which is the acceptor site for the CaM-binding domain: C_{537}ALLGFVT$_{544}$ (*16*).

The structure of the CaM/C20W complex may have special significance for the function of the Ca^{2+} pump. Differences in affinity of CaM have been described with respect to the two halves of the CaM-binding domain including various isoforms of the pump which differ in the C-terminal half of the CaM-binding domain due to alternative splicing (*23*). These variations result in different activation profiles of the pump and lead to the fine modulation of the pump by CaM (*14*, *18*, *75*, *77*) possibly influencing the apparent affinity of the enzyme for Ca^{2+} (*77*). As a consequence of the fact that the Ca^{2+}-loaded C-terminal domain alone activates the pump, we would expect that full CaM loaded with just two Ca^{2+} ions would bind and activate the pump as well. Such a conclusion is corroborated by experiments recently conducted on skMLCK (*78*). SAXS measurements provided evidence that a complex between skMLCK and CaM was formed already at $(Ca^{2+})_2$-CaM. Since Ca^{2+} binds first to the C-terminal half of CaM, those results would imply that for CaM-target interactions binding of Ca^{2+} to the C-terminal half of CaM would be sufficient. If this interpretation is also valid for the Ca^{2+} pump, we could conclude that a complex between CaM and the pump could be formed already at substoichiometric Ca^{2+} concentrations. Since, on the other hand, the C-terminal half of CaM is sufficient for the activation of the Ca^{2+} pump, the pump could be active (but at low efficiency) even at the low Ca^{2+} concentrations of the resting cell at which only the Ca^{2+} binding sites of the C-terminal half of CaM would be loaded in a CaM−Ca^{2+} pump complex. This view is in line with the observation that high-affinity binding of C20W to CaM occurs already at a stoichiometry of 2 Ca^{2+}/CaM at about 200 nM Ca^{2+} concentration (*79*) compatible with the free Ca^{2+} concentration of a resting cell and that intact Ca^{2+} binding sites of the C-terminal half of CaM are essential for the activation of the Ca^{2+} pump (*80*).

Thus the interaction between the C-terminal half of CaM and the CaM-binding domain of the pump would be

necessary (and sufficient) to release the autoinhibited state of the enzyme, but not for the full cooperativity typical of the system, thus providing a snapshot of the complex trapped in a step along its way to form the collapsed globular structure.

ACKNOWLEDGMENT

We thank M. Nilges, EMBL, Heidelberg, and H. Sticht, University of Bayreuth, for advice on structure calculation. We also thank K. M. Fiebig, Yale University, for drawing our attention to the program CALCROT to calculate SAXS data. This program was written by Ed Lattman, Johns Hopkins University, Baltimore, MD.

SUPPORTING INFORMATION AVAILABLE

Table S1 listing the NMR experiments with parameters, Table S2 containing the ^{1}H, ^{15}N, and ^{13}C chemical shift assignments for CaM, Table S3 containing the ^{1}H chemical shift assignment for the peptide C20W, and a figure showing the number of NOE restraints per residue. This material is available free of charge via the Internet at http://pubs.acs.org.

REFERENCES

1. Means, A. R. (1994) *FEBS Lett. 347*, 1−4.
2. Cohen, P., and Klee, C. B., Eds. (1988) in *Calmodulin. Molecular Aspects of Cellular Regulation*, Vol. 5, Elsevier, Amsterdam.
3. Zhang, M., Tanaka, T., and Ikura, M. (1995) *Nat. Struct. Biol. 2*, 758−767.
4. Kuboniva, H., Tjandra, N., Grzesiek, S., Ren, H., Klee, C. B., and Bax, A. (1995) *Nat. Struct. Biol. 2*, 768−776.
5. Krebs, J., Bürkler, J., Guerini, D., Brunner, J., and Carafoli, E. (1984) *Biochemistry 23*, 400−403.
6. Barbato, G., Ikura, M., Kay, L. E., Pastor, R. W., and Bax, A. (1992) *Biochemistry 31*, 5269−5278.
7. Ikura, M., Spera, S., Barbato, G., Kay, L. E., Krinks, M., and Bax, A. (1991) *Biochemistry 30*, 9216−9228.
8. Persechini, A., and Kretsinger, R. H. (1988) *J. Biol. Chem. 263*, 12175−12178.
9. Ikura, M., Clore, G. M., Gronenborn, A. M., Zhu, G., Klee, C. B., and Bax, A. (1992) *Science 256*, 632−638.
10. Meador, W. E., Means, A. R., and Quiocho, F. A. (1992) *Science 257*, 1251−1255.
11. Meador, W. E., Means, A. R., and Quiocho, F. A. (1993) *Science 263*, 1718−1721.
12. Babu, Y. S., Sack, J. S., Greenhough, T. J., Bugg, C. E., Means, A. R., and Cook, W. J. (1985) *Nature 315*, 37−40.
13. Clore, G. M., Bax, A., Ikura, M., and Gronenborn, A. (1993) *Curr. Opin. Struct. Biol. 3*, 838−845.
14. Carafoli, E. (1995) *FASEB J. 8*, 993−1002.
15. Verma, A. K., Filoteo, A. G., Stanford, D. R., Wieben, E. D., Penniston, J. T., Strehler, E. E., Fischer, R., Heim, R., Vogel, G., Mathews, S., Strehler-Page, M.-A., James, P., Vorherr, T., Krebs, J., and Carafoli, E. (1988) *J. Biol. Chem. 263*, 14152−14159.
16. Falchetto, R., Vorherr, T., Brunner, J., and Carafoli, E. (1991) *J. Biol. Chem. 266*, 2930−2936.
17. Falchetto, R., Vorherr, T., and Carafoli, E. (1992) *Protein Sci. 1*, 1613−1621.
18. Guerini, D., Krebs, J., and Carafoli, E. (1984) *J. Biol. Chem. 259*, 15172−15177.
19. Newton, D. L., Oldewurtel, M. D., Krinks, M. H., Shiloach, J., and Klee, C. B. (1984) *J. Biol. Chem. 259*, 4419−4426.
20. Barth, A., Martin, S. R., and Bayley, P. M. (1998) *J. Biol. Chem. 273*, 2174−2183.
21. Klumpp, S., Guerini, D., Krebs, J., and Schultz, J. E. (1987) *Biochem. Biophys. Res. Commun. 142*, 857−864.
22. Kuznicki, J., Grabarek, Z., Brzeska, H., Drabikowski, W., and Cohen, P. (1981) *FEBS Lett. 130*, 141−145,
23. Strehler, E. E. (1991) *J. Membr. Biol. 120*, 1−15.
24. Vorherr, T., James, P., Krebs, J., Enyedi, A., McCormick, D. J., Penniston, J. T., and Carafoli, E. (1990) *Biochemistry 29*, 355−365.
25. Trewhella, J. (1994) in *Structural Biology: The State of the Art* (Sarma, R. H., and Sarma, M. H., Eds.) Adenine Press, Guilderland, NY.
26. Kataoka, M., Head, J. F., Vorherr, T., Krebs, J., and Carafoli, E. (1991) *Biochemistry 30*, 6247−6251.
27. Chien, Y., and Dawid I. (1984) *Mol. Cell. Biol. 4*, 507−513.
28. Shatzman, A. R., and Rosenberg, M. (1987) *Ann. N.Y. Acad. Sci. 478*, 233−248.
29. Ikura, M. Kay, L. E., Krinks, M., and Bax, A. (1991) *Biochemistry 30*, 5498−5504.
30. Walsh, M., Stevens, F. C., Kuznicki, J., and Drabikowski, W. (1977) *J. Biol. Chem. 252*, 7440−7443.
31. Toda, H., Yazawa, M., Kondo, K., Honma, T., Narita, K., and Yagi, K. (1981) *J. Biochem. (Tokyo) 90*, 1493−1505.
32. Muhandiram, D. R., and Kay, L. E. (1994) *J. Magn. Reson. B 103*, 203−216.
33. Schleucher, J., Schwendinger, M., Sattler, M., Schmidt, P., Schedletzky, O., Glaser, S. J., Sørensen, O. W., and Griesinger, C. (1994) *J. Biomol. NMR 4*, 301−306.
34. Palmer, A. G., Cavanagh, J., Wright, P. E., and Rance, M. (1991) *J. Magn. Reson. 93*, 151−170.
35. Kay, L. E., Xu, G. Y., and Yamazaki, T. (1994) *J. Magn. Reson. A 109*, 129−133.
36. Marion, D., Ikura, M., Tschudin, R., and Bax, A. (1989) *J. Magn. Reson. 85*, 393−399.
37. Wishart, D. S., Bigam, C. G., Yao, J., Abildgaard, F., Dyson, H. J., Oldfield, E., Markley, J. L., and Sykes, B. D. (1995) *J. Biomol. NMR 6*, 135−140.
38. Bax, A., and Grzesiek, S. (1993) *Acc. Chem. Res. 26*, 131−138.
39. Grzesiek, S., Anglister, J., and Bax, A. (1993) *J. Magn. Reson. B 101*, 114−119.
40. Vuister, G. W., and Bax, A. (1993) *J. Am. Chem. Soc. 115*, 7772−7777.
41. Fesik, S. W., and Zuiderweg, E. R. P. (1988) *J. Magn. Reson. 78*, 588−593.
42. Fesik, S. W., Eaton, H. L., Olejniczak, E. T., Zuiderweg, E. R. P., McIntosh, L. P., and Dahlquist, F. W. (1990) *J. Am. Chem. Soc. 112*, 886−888.
43. Montelione, G. T., Lyons, B. A., Emerson, S. D., and Tashiro, M. (1992) *J. Am. Chem. Soc. 114*, 10974−10975; Lyons, B. A., and Montelione, G. T. (1993) *J. Magn. Reson. B101*, 206−209; Logan, T. M., Olejniczak, E. T., Zhu, R. X., and Fesik, S. W. (1993) *J. Biomol. NMR 3*, 225−231.
44. Carlomagno, T., Maurer, M., Sattler, M., Schwendinger, M. G., Glaser, S. J., and Griesinger, C. (1996) *J. Biomol. NMR 8*, 161−170.
45. Bax, A., Delaglio, F., Grzesiek, S., and Vuister, G. W. (1994) *J. Biomol. NMR 4*, 787−797.
46. Ikura, M., Kay, L. E., Tschudin, R., and Bax, A. (1990) *J. Magn. Reson. 86*, 204−209.
47. Zwahlen, C., Legault, P., Vincent, S. J. F., Greenblatt, J., Konrat, R., and Kay, L. E. (1997) *J. Am. Chem. Soc. 119*, 6711−6721.
48. Kuboniwa, H., Grzesiek, S., Delaglio, F., and Bax, A. (1994) *J. Biomol. NMR 4*, 871−878.
49. Hu, J.-S., Grzesiek, S., and Bax, A. (1997) *J. Am. Chem. Soc. 119*, 1803−1804.
50. Farrow, N. A., Muhandiram, R., Singer, A. U., Pascal, S. M., Kay, C. M., Gish, G., Shoelson, S. E., Pawson, T., Forman-Kay, J. D., and Kay, L. E. (1994) *Biochemistry 33*, 5984−6003.
51. Dayie, K. T., and Wagner, G. (1994) *J. Magn. Reson. A 111*, 121−126.
52. Boyd, J., Hommel, U., and Campbell, I. D. (1990) *Chem. Phys. Lett. 175*, 477.
53. Palmer, A. G., Skelton, N. J., Chazin, W. J., Wright, P. E., and Rance, M. (1992) *Mol. Phys. 75*, 699.
54. Kay, L. E., Nicholson, L. K., Delaglio, F., Bax, A., and Torchia, D. A. (1992) *J. Magn. Reson. 97*, 359.

55. Lipari, G., and Szabo, A. (1982) *J. Am. Chem. Soc. 104*, 4546−4559.
56. Lipari, G., and Szabo, A. (1982) *J. Am. Chem. Soc. 104*, 4559−4570.
57. Palmer, A. G., Rance, M., and Wright, P. E. (1991) *J. Am. Chem. Soc. 113*, 4371−4380.
58. Mandel, A. M., Akke, M., and Palmer, A. G. (1995) *J. Mol. Biol. 246*, 144−163.
59. Clore, G., Gronenborn, A., Nilges, M., and Ryan, C. (1987) *Biochemistry 26*, 8012−8023.
60. Wishart, D. S., Sykes, B. D., and Richards, F. M. (1991) *J. Mol. Biol. 222*, 311−333.
61. Deslauriers, R., and Smith, I. C. P. (1980) in *Biological Magnetic Resonance* (Berliner, L. J., and Reuben, J., Eds.) Vol. 2, pp 286−288, Plenum Press, New York.
62. Baxter, N. J., and Williamson, M. P. (1997) *J. Biomol. NMR 9*, 359−369.
63. Osawa, M., Swindells, M. B., Tanikawa, J., Tanaka, T., Mase, T., Furuya, T., and Ikura, M. (1998) *J. Mol. Biol. 276*, 165−176.
64. Brünger, A. T. (1992) *X-PLOR: A System for X-ray Crystallography and NMR*, Yale University Press, New Haven, CT.
65. Konradi, R., Billeter, M., and Wüthrich, K. (1996) *J. Mol. Graphics 14*, 51−55.
66. Ikura, M., Kay, L. E., and Bax, A. (1990) *Biochemistry 29*, 4659−4667.
67. O'Neil, K. T., and DeGrado, W. F. (1990) *Trends Biochem. Sci. 15*, 59−64.
68. Siivari, K., Zhang, M., Palmer, A. G., III, and Vogel, H. J (1995) *FEBS Lett. 366*, 104−108.
69. Laskowski, R. A., Rullmann, J. A. C., MacArthur, M. W., Kaptein, R., and Thornton, J. M. (1996) *J. Biomol. NMR 8*, 477−486.
70. Nilges, M., and O'Donoghue, S. I. (1998) *Prog. NMR Spectrosc. 32*, 107−139.
71. Case, D. A. (1995) *J. Biomol. NMR 6*, 341−346.
72. Gellman, S. H. (1991) *Biochemistry 30*, 6633−6626.
73. Chin, D., Winkler, K. E., and Means, A. R. (1997) *J. Biol. Chem. 272*, 31235−31240.
74. Guerini, D., Krebs, J., and Carafoli, E. (1987) *Eur. J. Biochem. 170*, 35−42.
75. Vorherr, T., Quadroni, M., Krebs, J., and Carafoli, E. (1992) *Biochemistry 31*, 8245−8251.
76. Goldberg, J., Nairn, A. C., and Kuriyan, J. (1996) *Cell 84*, 875−887.
77. Enyedi, A., Verma, A. K., Heim, R., Adamo, H. P., Filoteo, A. G., Strehler, E. E., and Penniston, J. P. (1994) *J. Biol. Chem. 269*, 41−43.
78. Krueger, J. K., Bishop, N. A., Blumenthal, D. K., Zhi, G., Beckingham, K., Stull, J. T., and Trewhella, J. (1998) *Biochemistry 37*, 17810−17817.
79. Yazawa, M., Vorherr, T., James, P., Carafoli, E., and Yagi, K. (1992) *Biochemistry 31*, 3171−3176.
80. Gao, Z. H., Krebs, J., Van Berkum, M. F. A., Tang, W.-J., Maune, J. F., Gilman, A. G., Means, A. R., Stull, J. T., and Beckingham, K. (1993) *J. Biol. Chem. 268*, 20096−20104.

BI9908235